International Journal of Nanomedicine

Dovepress
Taylor & Francis Group

Open Access Full Text Article

ORIGINAL RESEARCH

LbL-Antibody Embedded Gold Mesh: An Effective Method for Early Detection of Circulating Tumor Cells

Rong Qin[1,2], Zhihao Ma[3], Chenglong Song[3], Chenghong Huang[4], Zhiqiang Zhu[5], Jing Yan[6], Jie Wang[3]

[1]Department of Medical Oncology, Jiangsu University Affiliated People's Hospital, Zhenjiang, People's Republic of China; [2]Zhenjiang Clinical Medical College of Nanjing Medical University, Zhenjiang, People's Republic of China; [3]Institute for Advanced Materials, School of Materials Science and Engineering, Jiangsu University, Zhenjiang, 212013, People's Republic of China; [4]Chongqing university of Science and Technology, Chongqing, 401331, People's Republic of China; [5]Suzhou Chien-Shiung Institute of Technology, Suzhou, 215123, People's Republic of China; [6]Holosensor Medical Ltd., Suzhou, 215000, People's Republic of China

Correspondence: Jie Wang; Jing Yan, Email wangjie@ujs.edu.cn; yj@hemosmartmed.com

Introduction: The importance of early cancer diagnosis has been recognized for decades, driving the demand for technological advancements and novel strategies for cancer detection. The conventional detection of circulating tumor cells (CTCs) often relies on size-based separation to distinguish CTCs from other blood cells. However, this method frequently leads to significant cell congestion and poorly recognizable fluorescent images, which inevitably reduces the sensitivity and specificity of CTC detection. Most CTC current separation devices with a cell filtration process have a cell capture efficiency ranging from 50% to 80% in clinical application.

Methods: We constructed a flexible antibody network on the surface of gold-plated iron meshes with a pore size of 20 μm using the layer-by-layer (LbL) assembly technique. These meshes were then used to enrich MCF7 cells and CTCs in 10 clinical blood samples from breast cancer patients.

Results and the Conclusion: This antibody network reduced the effective pore size, thereby improving both capture efficiency and specificity for CTCs. In a cell line separation study, meshes with a trilayered antibody network demonstrated a capture efficiency of 65% compared to 26% for those with a single layer. In tests using clinical samples, the trilayered antibody network achieved 100% accuracy, whereas the single-layer configuration only reached 40%. The multilayered antibody network shows strong potential for enhancing widely used immunosensors.

Keywords: circulating tumor cells, CTCs, immunosensor, layer-by-layer assembly, LbL

Introduction

Currently, cancer-related illnesses are among the most serious health challenges worldwide. Research on effective techniques for early diagnosis and treatment is therefore critically important. The routine clinical treatment of patients with cancer undergoing surgery, chemotherapy, and radiotherapy underestimates inter- and intra-patient heterogeneity. To address this issue, personalized early diagnosis in precision oncology is indispensable.[1] Early diagnostic and prognostic technologies are gradually shifting from conventional to more sophisticated techniques,[2–5] including the detection of circulating tumor cells (CTCs).[6,7] CTCs originate from primary tumor sites and circulate in the peripheral blood, making them promising biomarkers for cancer diagnoses. These cells can be detected as early as 4–6 months before traditional PET/CT imaging.[8] Detecting CTCs could serve as an effective early-diagnosis tool combined with conventional tumor detection methods. CTC-based techniques are considerably less invasive and can provide valuable prognostic information regarding treatment efficacy. However, the scarcity of CTCs presents a considerable challenge for detection technologies, demanding high sensitivity.[9–12] Most current CTC separation devices rely on the size distinction between CTCs and other cells. The process of isolating circulating tumor cells (CTCs) through filtration often leads to significant cell congestion and yields unclear fluorescence images. These issues contribute to reduced sensitivity—typically ranging

Received: 9 May 2025
Accepted: 17 September 2025
Published: 10 November 2025

from 50% to 80%—and low specificity,[13–18] ultimately limiting the reliability and broader applicability of CTC detection. Theoretically, too small pores used in cell filtration lead to cell clogging and reduced specificity, while overly large pores result in a low sensitivity. Fixed-pore-size filters struggle to meet both demands of high sensitivity and excellent specificity. Based on this principle, CTC sensors could be improved through the use of flexible pore structures.

In the construction of immunosensors, capture antibodies are typically immobilized using techniques such as glutaraldehyde (Glu) cross-linking, cysteamine hydrochloride (CH), or EDC/NHS chemistry, which generally result in the formation of a monolayer of antibodies on the immunosensor.[19,20] However, such a configuration inherently limits the antibody loading capacity due to the constrained surface area. Moreover, antibodies are immobilized within nanometers of the sensor surface, which may restrict their molecular flexibility and hinder efficient binding to target antigens. According to previous studies, ligands featuring flexible spacer arms can enhance the mobility of immobilized antibodies, thereby improving capture efficiency, particularly at low analyte concentration.[21]

In this study, we developed a cell separation device for capturing tumor cells from peripheral blood samples using a flexible multilayer antibody network. As illustrated in Figure 1, the device features a gold-plated iron mesh with pore sizes of 20 μm, functionalized via layer-by-layer (LbL) assembly of streptavidin and biotin-labeled antibodies. Unlike conventional sensors with monolayer antibody coverage, this approach constructs a soft and flexible recognizing molecules layer on the rigid mesh substrate. This flexible architecture not only enhances molecular recognition but

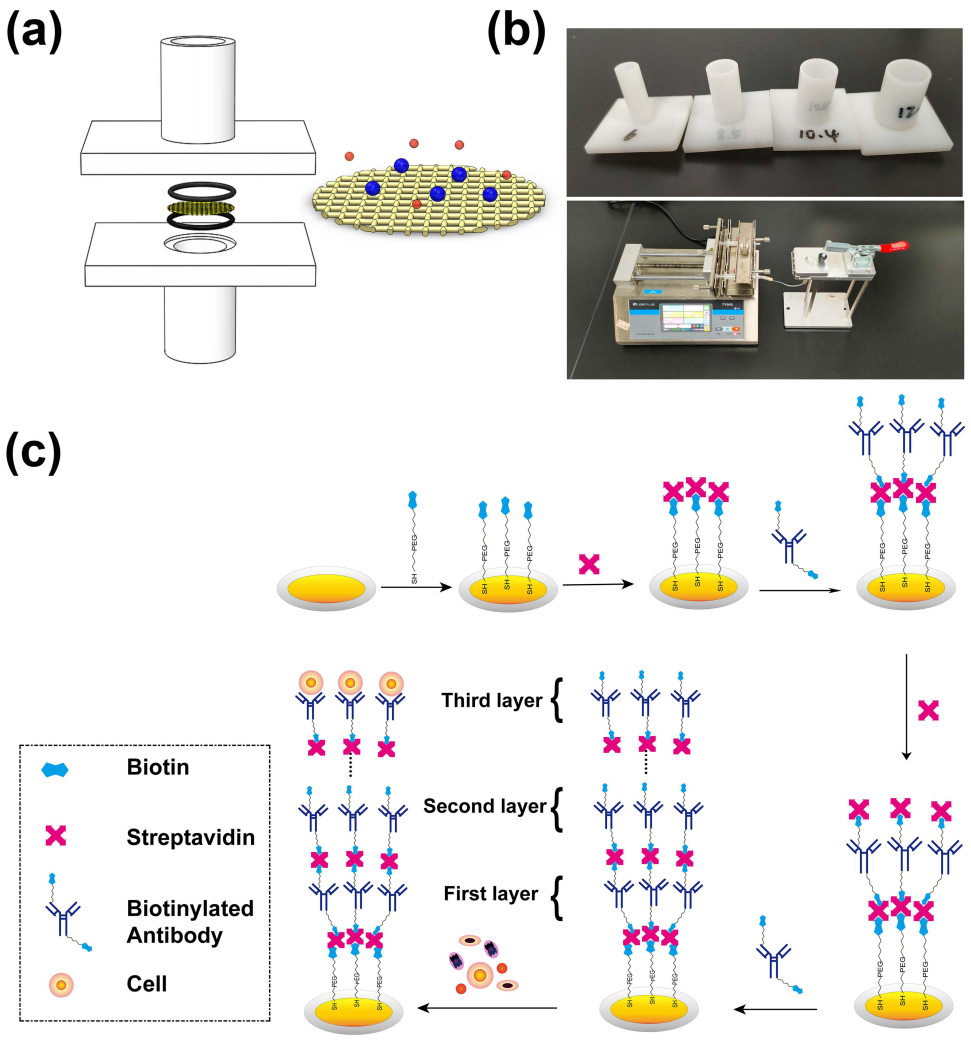

Figure 1 Schematic of an CTCs separation platform based on LbL assembly of antibody. (**a**) Exploded view of the filtration unit, consisting of a gold-plated mesh secured within a Teflon holder; (**b**) 3D-printed holder and its connection with a syringe pump; (**c**) The workflow of the Layer-by-Layer (LbL) process used to fabricate a three-dimensional (3D) network of anti-EpCAM antibodies on the gold-coated surface.

also effectively reduced the functional pore size during filtration. As a result, the device achieves an improved balance between high sensitivity and specificity in circulating CTCs detection.

Materials and Methods

Biotin-labelled HS-PEG(5000) was purchased from Ponsure Biotechnology Co., Ltd. (China). TCEP and streptavidin were purchased from Sigma-Aldrich company (USA). Biotin-labelled anti-EpCAM antibody was purchased from BioLegend (USA). All other chemicals were of analytical grade and all aqueous solutions were prepared using deionized water.

1mM Tris (2-carboxyethyl) phosphine (TCEP) solution was prepared by dissolving 0.5 mg TCEP powder in 1.75mL PBS. HS-PEG(5000)-biotin powder was dissolved in TCEP solution to obtain a 1mM HS-PEG(5000)-biotin solution. HS-PEG(5000)-biotin solution was then added onto the gold surface of the Quartz Crystal Microbalance (QCM) chip and incubated at room temperature for more than 10 h. Anti-human 326 (EpCAM), anti-Pan-CK, and anti-CD45 antibodies were purchased from BioLegend (San Diego, CA, USA), and DAPI was purchased from Merck (Darmstadt, Germany).

Blood samples of breast tumor patients were from Jiangsu University Affiliated People's Hospital. All procedures performed in studies involving human participants were in accordance with the ethical standards of the institutional research committee and the 1964 Helsinki Declaration and its later amendments. The study protocol was approved by the Ethics Committee of Jiangsu University Affiliated People's Hospital (Approval No. K-20240039-W).

Preparation of Anti-EpCAM Antibody on Gold Surface

We constructed different layers of anti-EpCAM antibodies through the interaction of streptavidin and biotinylated anti-EpCAM antibodies. First, the HS-PEG(5000)-biotin solution was added to the gold surface and incubated for 10 h. 0.5 mg/mL streptavidin solution and biotin labelled anti-EpCAM antibody solution (≈33 pmoL/L) were successively incubated with the gold surface for 1 h to establish a single layer of the antibody. Finally, the gold surface was rinsed with PBS solution for 10 min. To construct multilayers of antibodies on the mesh, incubations with streptavidin solution and biotin-labelled antibodies were repeated alternately for three cycles, as illustrated in Figure 1.

Cell Culture Studies Using MCF-7 Cells

The MCF-7 cells were purchased from National Collection of Authenticated Cell Cultures (Shanghai, China) and cultured under well-known conditions. The basic medium for MCF-7 cells was MEM supplemented with 10% fetal bovine serum (FBS) and a combination of penicillin and streptomycin. MCF-7 cells were prestained with the intracellular fluorescent dye CFSE to simplify their counting.

Quartz Crystal Microbalance Measurement

QCM experiments were performed using Qsense E4 (Biolin Scientific, Sweden). In off-line experiments, QCM chips were placed in a 24-well microplate and incubated in 500μL of 0.5 mg/mL streptavidin solution and 10μL biotin-labelled anti-EpCAM antibody solution alternately to construct a single layer (single-cycle) or multilayer (multi-cycle) antibody assembly. The resonant frequency in air was recorded and analyzed before and after the LbL assembly. Antibody-modified QCM chips were used to capture MCF-7 cells, and the resonant frequency in air was recorded. In the online experiments, the QCM chips were mounted into a QCM chamber and the corresponding frequency change was monitored online.

Atomic Force Microscopy

Atomic force microscopy (AFM) images were obtained using a Multimode 8 apparatus (Bruker, USA) in the tapping mode with silicon cantilevers purchased from Olympus. The resonant frequency was set to 300kHz and the scan frequency was set to 1 Hz. The resolution of the AFM images was set at 512 × 512 pixels. Gold surfaces covered by a single layer and a three-layer anti-EpCAM antibody were characterized by AFM in air.

Electrochemical Measurement

Electrochemical measurements were performed on a Chenhua electrochemical workstation (CHI660E) with 5mM $K_3[Fe(CN)_6]/K_4[Fe(CN)_6]$ as the redox probe in a 0.1M KCl solution. A traditional three-electrode system was employed,

consisting of a gold electrode as the working electrode, Ag/AgCl electrode as the reference electrode, and platinum wire electrode as the counter electrode.

All working electrodes were immersed in piranha solution (70% concentrated sulfuric acid and 30% H_2O_2) for 30 min and then washed with distilled water. After that, the electrodes were polished with 0.3μm and 0.05μm alumina and then sonicated in ethanol and deionized water in sequence. After drying with nitrogen, the electrodes were placed in a freshly prepared 0.5M sulfuric acid solution. Cyclic voltammetry (CV) and Electrochemical impedance spectroscopy (EIS) curves were recorded with the voltage shifting from −0.4V to 1.6V.

Cell Enrichment Studies Using the Gold Meshes Modified with Anti-EpCAM Antibody

A gold-plated iron mesh was used for the enrichment of MCF-7 cells. An LbL-assembled 3D anti-EpCAM antibody network was constructed on the gold surface of meshes and subsequently used to capture MCF-7 cells from Jurkat cells, which served as the background cells. To test the efficacy of the CTC platform, 200 μL (100,000 cells/mL) of a cell suspension containing 20,000 CFSE-labeled MCF-7 cells was processed through meshes at a rate of 25 μL/min and counted. To capture trace cells, 100 CFSE-labeled MCF-7 cells were captured and compared based on a single-layer antibody-functionalized mesh and a trilayer antibody-functionalized mesh. A mixture of 18 MCF-7 cells (EpCAM-positive) and 5106 Jurkat cells (EpCAM-negative) was pushed through the meshes modified with different layers of anti-EpCAM antibody. MCF-7 and Jurkat cells captured on the meshes were immunostained successively with anti-pan-CK, anti-CD45 antibodies, and DAPI solution.

Circulating Tumor Cells Detection from the Clinical Samples

About 12 mL peripheral blood samples from 10 breast cancer patients were collected with Clinical characteristics of the patients included in Table S1 of supporting information. Peripheral blood mononuclear cells (PBMC) were obtained after processing by typical density gradient centrifugation. Subsequently, cells were pushed through a gold mesh for CTCs detection.

Results and Discussion

It is well known that the low abundance of CTCs and the interference from millions of peripheral blood mononuclear cells (PBMCs) in blood samples are the main challenges for CTC-based techniques. These challenges often lead to cell congestion at the filtration pores of size-based devices. Consequently, high specificity in such devices is usually accompanied by low CTC capture efficiency. Theoretically, flexible pore structures can expand under pressure, allowing PBMCs to pass through more readily than rigid pores of the same size. This deformability helps minimize clogging and enables high specificity while maintaining high CTC capture efficiency. Moreover, the soft and flexible nature of such pores helps to preserve the integrity of captured cells, reducing the risk of membrane damage.

As shown in Figure 1c, a flexible 3D antibody film was fabricated on gold-plated iron meshes using a LbL assembly approach based on streptavidin–biotin interactions. This design increases the loading capacity of capture antibodies and provides greater spatial flexibility. The modification process began with the self-assembly of HS-PEG(5000)-biotin on the gold substrate, followed by iterative incubation with streptavidin and biotin-labeled anti-EpCAM antibody to form a multilayered architecture. The anti-EpCAM antibody was used as the capture antibody for CTCs. The performance of this CTC separation platform was evaluated using both MCF-7 cell line and clinical blood samples.

The QCM is a well-known mass sensor based on the piezoelectric effect. The resonance frequency of the QCM decreases as the mass on the sensor surface increases. In liquid environments, the viscoelastic properties and thickness changes of analytes layers can be analyzed by simulation using the Voigt model. In this study, the QCM was used to monitor the construction of an antibody network via LbL assembly. The LbL process was first investigated offline in air. The frequency shift at the third overtone (ΔF_3) was recorded to analyze the formation of the anti-EpCAM antibody. Streptavidin, which forms a tetramer capable of binding up to four biotin molecules, theoretically enables an increase in antibody immobilization with each added layer. The ΔF_3 difference induced by immobilizing a single layer and a three-layer antibody in air was 1840 Hz (F_3 was 14983310 Hz and 14985158 Hz for a single and three-layer antibody, respectively). According to the Sauerbrey Equation, which relates resonant frequency shift to mass change on the QCM crystal surface,[22,23] the mass sensitivity for a 5 MHz fundamental frequency crystal is –17.7 ng cm^{-2} Hz^{-1}. Using

Equation (1), a frequency shift of 1840 Hz corresponds to a mass change of 10.9 μg/cm^{-2} on the QCM chip surface, which confirms the enhanced antibody immobilization by LbL multilayer assembly.

$$= -C \times \Delta f / n \tag{1}$$

Subsequently, the LbL assembly process of the antibody in the liquid was monitored in real time. As shown in Figure 2a, the immobilization of a single antibody layer on the QCM chip resulted in a frequency shift of 33.8 ± 2.5 Hz. Streptavidin and anti-EpCAM antibody solutions were then pumped into the QCM chamber iteratively three times to form a three-layer assembly. As shown in Figure 2b, the stepwise changes in both resonant frequency and energy dissipation curves indicated the successful construction of the multilayer antibody architecture through repetitive streptavidin–biotin interactions. The frequency shift for a three-layer antibody assembly was 78.2 ± 5.8 Hz, much higher than that of a single layer of antibody. To evaluate capture performance, a mixed cell suspension containing MCF-7 and Jurkat cells was pumped into the chamber. As shown in Figure 2c–d, the frequency shifts induced by cell capture were 3.8 ± 2.5 Hz for the single-layer antibody and 16.2 ± 5.8 Hz for the three-layer system, indicating enhanced MCF-7 capture with the multilayer assembly. The energy dissipation signals further revealed a stronger modulation of substrate viscoelasticity by cells captured with the three-layer antibody, suggesting the presence of a larger number of cells and possibly a thicker cellular layer on the surface. In conclusion, QCM analysis suggests that the LbL-assembled multi-layered antibody network captured more MCF-7 cells compared to the single-layer configuration.

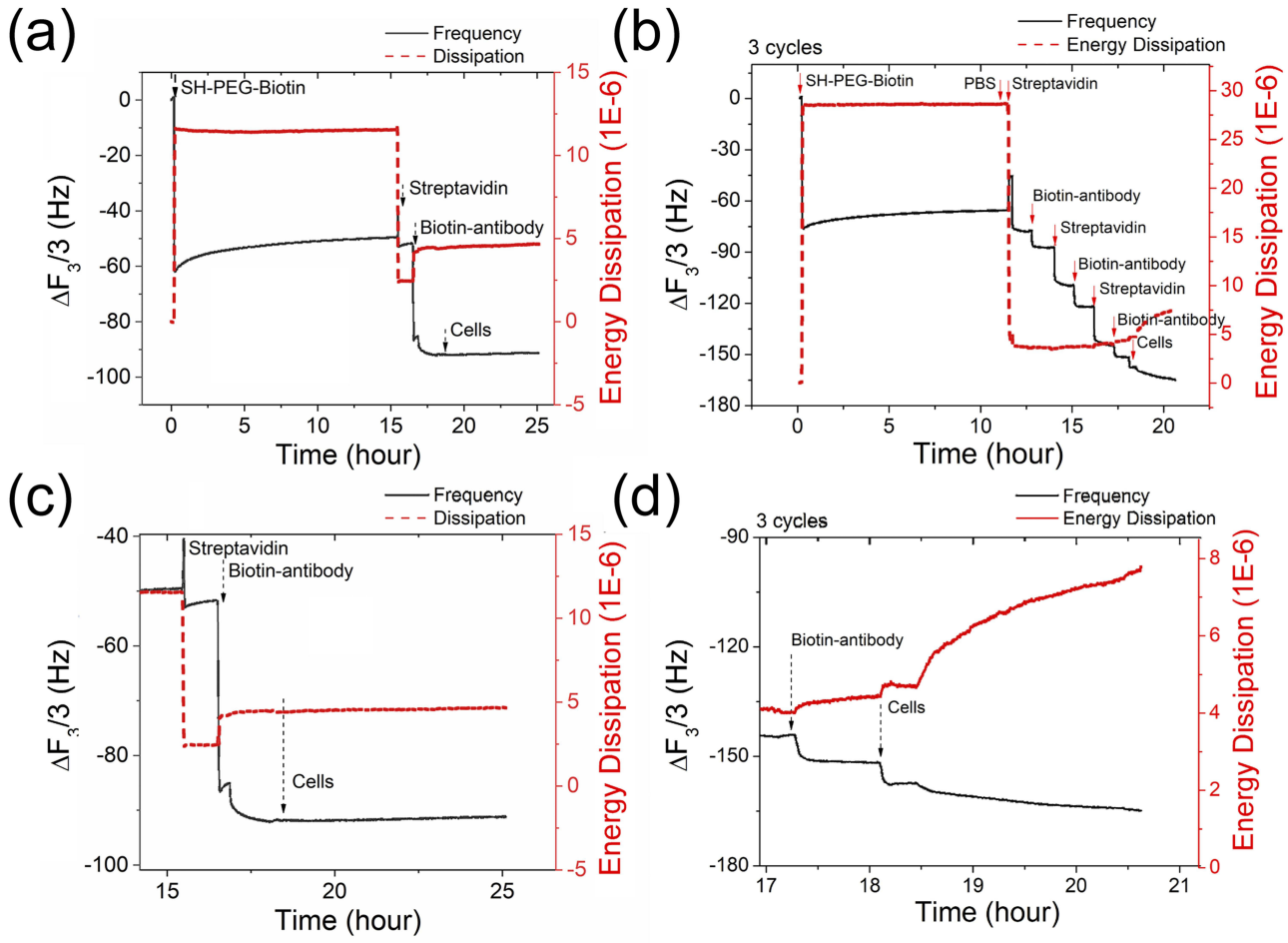

Figure 2 Resonant frequency and energy dissipation curves for (**a**) formation of a single antibody layer; (**b**) formation of a three-layer antibody assembly; (**c**) cell capture by a single antibody layer; (**d**) cell capture by a three-layer antibody. The red and black colored dotted arrows with text indicated the addition of streptavidin and biotinylated antibody respectively, during the LbL assembly process.

https://doi.org/10.2147/IJN.S529248

AFM was used to characterize the morphology of the assembled anti-EpCAM antibody layers. As shown in Figure 3, height measurements of the bare gold substrate (2.7 ± 0.3 nm), a single antibody layer (8.8 ± 2.5 nm), and a three-layer antibody assembly (14.4 ± 3.7 nm) confirmed the successful construction of LbL film on the surface. Furthermore, AFM topographical analysis in Figure 3b reveals distinct morphological transitions: single-layer antibodies form a sparse network of interconnected fibrillar structures, whereas the three-layer assembly produces a continuous and densely packed film on the gold substrate.

The LbL assembly process and its effect on cell capture performance were further investigated by EIS measurements. As shown in Figure 4a, the electron transfer resistance (Ret) gradually increased during the LbL assembly of antibodies on the gold electrode surface, which was consistent withthe assumption that the deposition of biomolecules hindered electron transfer to the electrode. As shown in Figure 4b, a significant increase in Ret was observed after the formation of the first antibody layer. The impedance showed a gradual increase from the formation of the first, second, and third antibody layers, suggesting the successful stepwise assembly of the multilayered structure. The cells captured on the electrode surface with two or three antibody layers induced impedance increment of 3.39×10^5 Ω and 5.55×10^5 Ω,

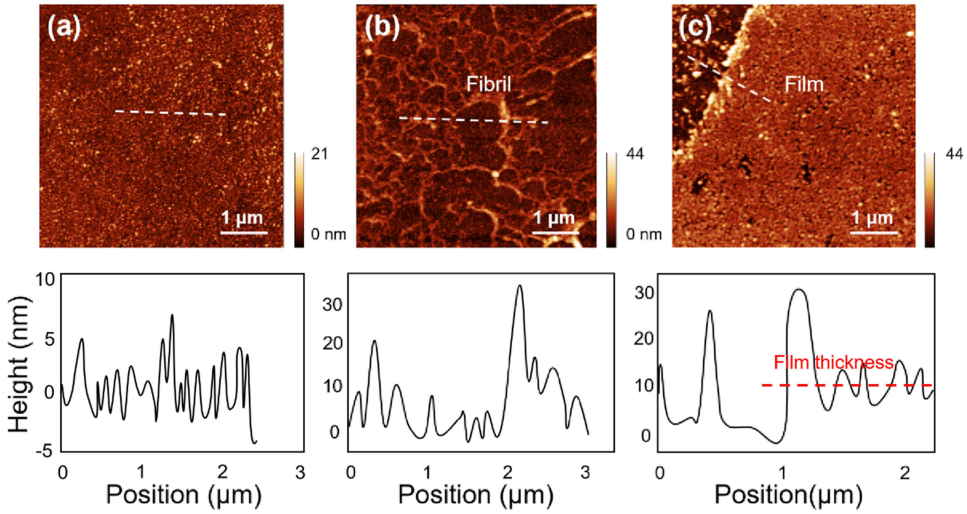

Figure 3 AFM images of (**a**) bare gold surface; (**b**) gold substrate modified with a single-layer of anti-EpCAM antibody; (**c**) gold substrate modified with a three-layer of anti-EpCAM antibody. The white dotted lines indicate the location of height profiles.

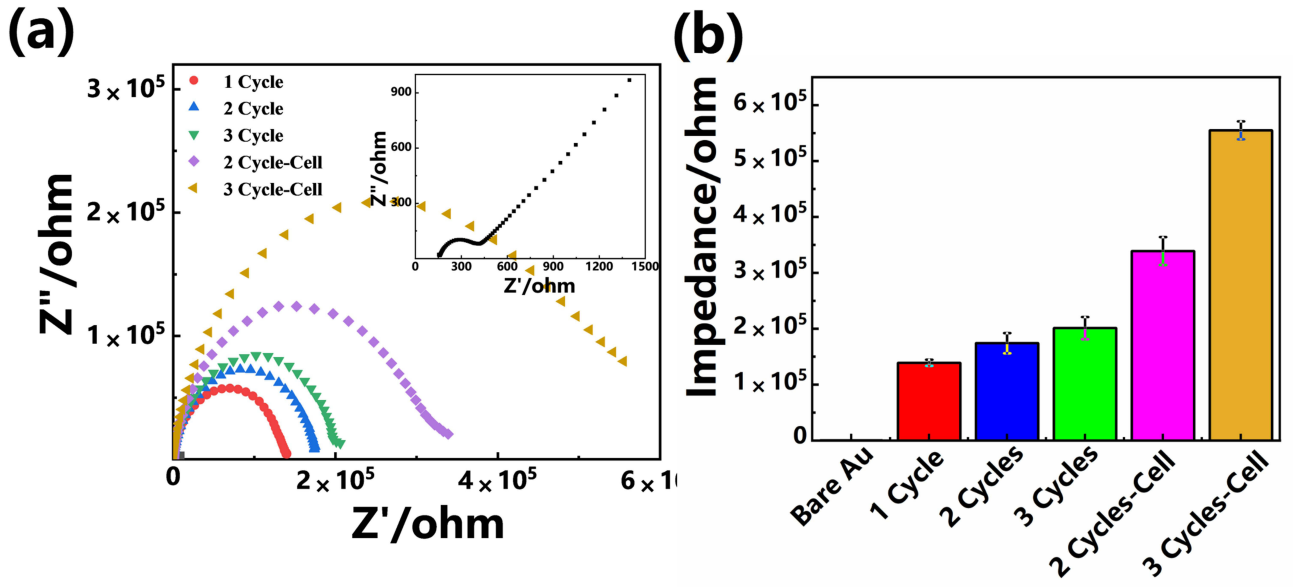

Figure 4 (**a**) EIS curves and (**b**) R_{et} value for gold electrodes modified with varying numbers of anti-EpCAM antibody layers, before and after cell capture.

respectively. These electrochemical measurements indicated that the multilayered anti-EpCAM antibody enhanced the cell capture performance compared with the single-layer antibody.

A cell mixture containing target MCF-7 and Jurkat cells was employed as a model for CTCs and white blood cells, according to previous CTC studies.[24,25] A three-layer anti-EpCAM antibody network was immobilized onto gold-plated iron meshes with a pore size of 20 μm (Figure 1) to separate MCF-7 cells (EpCAM-positive) from Jurkat cells (EpCAM-negative). As illustrated in Figure 1, the iron meshes were secured in a 3D-printed teflon holder and connected to a syringe. Prior to capture, MCF-7 cells were prestained with intracellular fluorescent dye CFSE to facilitate cell counting and efficiency calculation. Under continuous flow conditions (25 μL/min), a suspension of CFSE-labeled MCF-7 cells (200 μL, 100,000 cells/mL) was processed through the functionalized meshes. The typical cell fluorescent images are shown in Figure 5a, and capture efficiency of 69.8 ± 2.1% was achieved. Figure 5b–c further demonstrates the

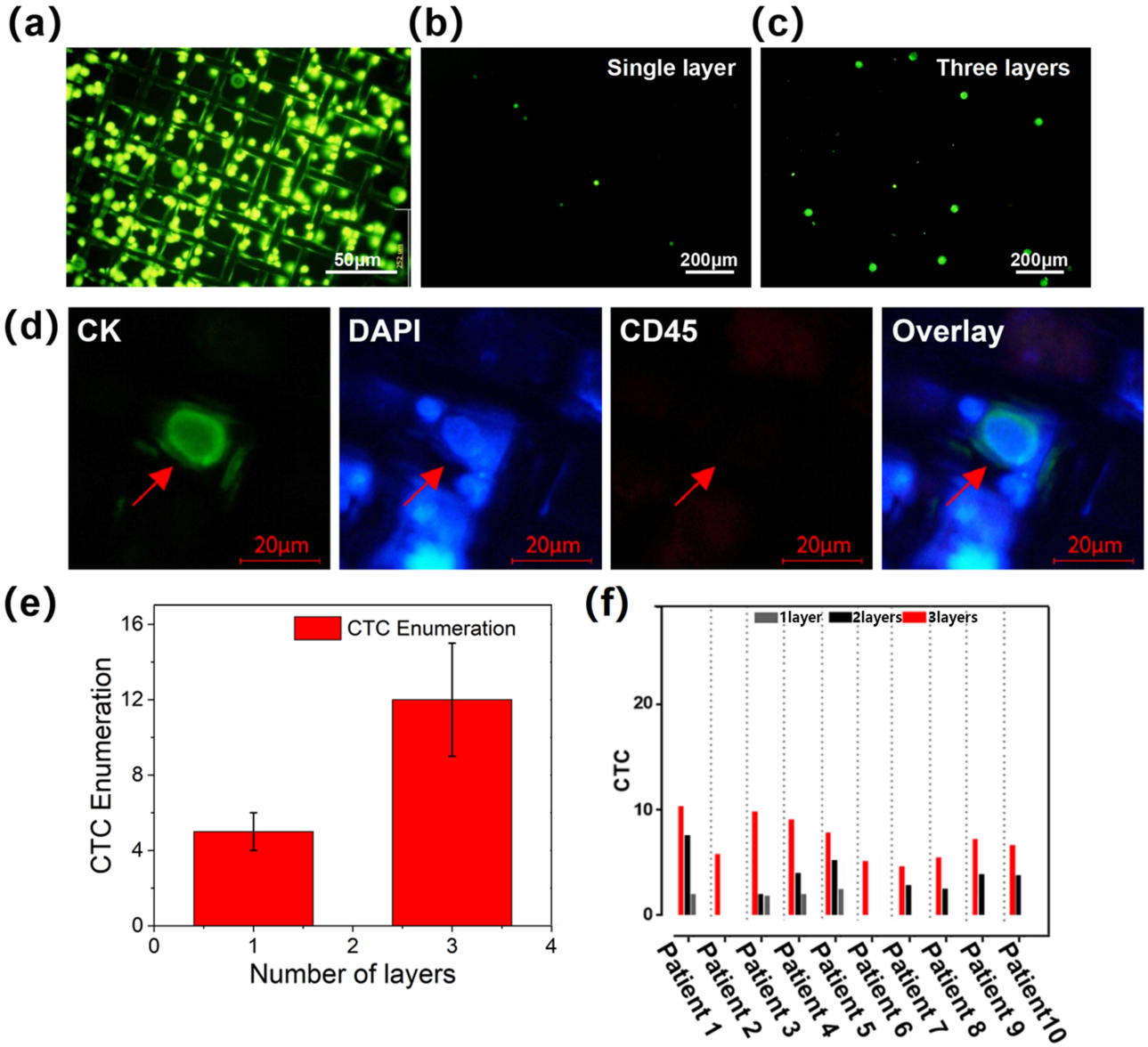

Figure 5 Evaluation of cell capture performance. (**a**) Fluorescent images 10,000 CFSE-prestained MCF-7 cells captured on the functionalized mesh; Fluorescent images of 100 CFSE-prestained MCF-7 cells captured using a single-layer (**b**) and a three-layer (**c**) antibody-functionalized mesh; (**d**) Immunostaining of captured MCF-7 cells (spiked into Jurkat cell background) with anti-pan-CK, anti-CD45, and DAPI; (**e**) Enumeration of captured and immunostained CTCs on meshes functionalized with different numbers of antibody layers; (**f**) Capture of CTCs from clinical patient samples using meshes modified with one-, two-, or three-layer antibody assemblies. CTC counts are represented by gray, black, and red bars, respectively.

https://doi.org/10.2147/IJN.S529248

performance of the trilayer antibody-modified platform in capturing 100 CFSE-labeled MCF-7 cells. The trilayer antibody-functionalized mesh captured 65 ± 8 cells compared with 26 ± 4 cells using a single-layer antibody system. Next, a cell mixture containing 18 MCF-7 cells and 5×10^6 Jurkat cells was processed through the platform, followed by in situ immunostaining with anti-pan-CK, anti-CD45 antibodies, and DAPI (Figure 5d). The immunostaining image showed successful identification of MCF-7 cells (pan-CK +, CD45 −, DAPI+). As shown in Figure 5e, the trilayer antibody-functionalized mesh captured 12 ± 3 cells, whereas the single-layer antibody system captured 5 ± 1 cells. The results demonstrated that the capture efficiency was enhanced by more layers of antibody assembly, due to higher antibody density and improved structural flexibility. The performance of this LbL-based CTCs sensor was compared with other technologies for CTC enrichment in Table S2 in supporting information.

Finally, multilayered antibody-functionalized meshes were used to capture CTCs from blood samples of breast tumor patients at Jiangsu University Affiliated People's Hospital. We collected 12 mL of blood from 10 patients with breast cancer and used meshes functionalized with one, two, or three layers of anti-EpCAM antibody to capture CTCs. As shown in Figure 5f, the numbers of CTCs captured by meshes with three, two, and one antibody layers are represented by red, black, and gray bars, respectively. Quantitative analysis revealed an enhancement in CTC capture efficiency with a trilayer antibody network compared with monolayer systems. Clinically significant detection was achieved exclusively by the trilayer functionalized meshes for all the patients, while monolayer counterparts showed 4 successful capture. These results established a direct correlation between the antibody network and clinical detectability.

Conclusion

In conclusion, we have developed a CTC separation platform based on gold-coated iron meshes functionalized with a multilayered antibody network. This multilayer architecture demonstrated the potential to enhance CTC capture efficiency. In tests using clinical samples, the three-layer antibody network achieved nearly 100% detection accuracy, compared to only 40% with a single-layer configuration. As the number of antibody layers increases, the resulting antibody network becomes both thicker and more flexible, contributing to improved capture performance. However, the number of layers may need further optimization, since excessively thick films may detach from the substrate. This multilayer antibody strategy shows potential for application in other immunosensor platforms.

Acknowledgments

This paper has been uploaded to SSRN as a preprint: [https://papers.ssrn.com/sol3/papers.cfm?abstract_id=4125830].

Author Contributions

All authors made a significant contribution to the work reported, whether that is in the conception, study design, execution, acquisition of data, analysis and interpretation, or in all these areas; took part in drafting, revising or critically reviewing the article; gave final approval of the version to be published; have agreed on the journal to which the article has been submitted; and agree to be accountable for all aspects of the work.

Funding

This research was funded by the Natural Science Foundation of Jiangsu Province (Grant no. 20150490) and the Science and Technology Program of Suzhou (SYW2025037). We acknowledge the financial support from the Research Project of Jiangsu University Affiliated People's Hospital (YP2023005, BJRH-2024-3) and the Project of Zhenjiang City Social Development (SH2023046).

Disclosure

The authors declare no competing interest in this work.

References

1. Yang C, Xia B-R, Jin W-L, Lou G. Circulating tumor cells in precision oncology: clinical applications in liquid biopsy and 3D organoid model. *Cancer Cell Int*. 2019;19:341. doi:10.1186/s12935-019-1067-8

2. Langer A. A systematic review of PET and PET/CT in oncology: a way to personalize cancer treatment in a cost-effective manner? *BMC Health Serv Res*. 2010;10(1):1–16. doi:10.1186/1472-6963-10-283
3. Mcdermott U, Settleman J. Personalized cancer therapy with selective kinase inhibitors: an emerging paradigm in medical oncology. *J Clin Oncol*. 2009;27(33):5650–5659. doi:10.1200/JCO.2009.22.9054
4. Assaraf YG, Leamon CP, Reddy JA. The folate receptor as a rational therapeutic target for personalized cancer treatment, drug resist. *Update*. 2014;17:89–95.
5. Agarwal A, Balic M, El-Ashry D, et al. Circulating tumor cells strategies for capture, analyses, and propagation. *Cancer J*. 2018;24(2):70–77. doi:10.1097/PPO.0000000000000310
6. Yue M, Li Y, Xing H, Luo M, Li Z. Circulating tumor cells: from theory to nanotechnology-based detection. *Front Pharmacol*. 2017;08:35.
7. Esmaeilsabzali H, Beischlag TV, Cox ME, Parameswaran AM, Park EJ. Detection and isolation of circulating tumor cells: principles and methods. *Biotechnol Adv*. 2013;31(7):1063–1084. doi:10.1016/j.biotechadv.2013.08.016
8. Bankó P, Sun YL, Nagygyörgy V, Zrínyi M, Telekes A. Technologies for circulating tumor cell separation from whole blood. *J Hematol Oncol*. 2019;12(1):48. doi:10.1186/s13045-019-0735-4
9. Meng S. Circulating Tumor Cells in patients with breast cancer dormancy. *Clin Cancer Res*. 2004;10:8152–8162.
10. Lin D, Shen L, Luo M, et al. Circulating tumor cells: biology and clinical significance. *Signal Transduct Tar*. 2021;6:404.
11. Prasanna BK, Balakrishnan A, Kumar P. Circulating tumor cell clusters and circulating tumor cell-derived explant models as a tool for treatment response. *BioTechniques*. 2020;69(1):4–5. doi:10.2144/btn-2020-0029
12. Kowalik A, Kowalewska M, Góźdź S. Current approaches for avoiding the limitations of circulating tumor cells detection methods—implications for diagnosis and treatment of patients with solid tumors, Transl. *Res*. 2017;185:58–84.e15.
13. Nagrath S, Sequist L, Maheswaran S, et al. Isolation of rare circulating tumour cells in cancer patients by microchip technology. *Nature*. 2007;450 (2007):1235–1239. doi:10.1038/nature06385
14. Jan YJ, Chen JF, Zhu Y, et al. NanoVelcro rare-cell assays for detection and characterization of circulating tumor cells. *Adv Drug Deliv Rev*. 2018;125(2018):78–93. doi:10.1016/j.addr.2018.03.006
15. Yoon HJ, Kim TH, Zhang Z, et al. Sensitive capture of circulating tumour cells by functionalized graphene oxide nanosheets. *Nat Nanotechnol*. 2013;8(2013):735–741. doi:10.1038/nnano.2013.194
16. Gleghorn JP, Pratt ED, Denning D, et al. Capture of circulating tumor cells from whole blood of prostate cancer patients using geometrically enhanced differential immunocapture (GEDI) and a prostate-specific antibody. *Lab Chip*. 2010;10(1):27–29. doi:10.1039/B917959C
17. Tang M, Wen C, Wu L, et al. A chip assisted immunomagnetic separation system for the efficient capture and in situ identification of circulating tumor cells. *Lab Chip*. 2016;16(2016):1214–1223. doi:10.1039/C5LC01555C
18. Chu C, Liu R, Ozkaya-Ahmadov T, et al. Hybrid negative enrichment of circulating tumor cells from whole blood in a 3D-printed monolithic device. *Lab Chip*. 2019;19(2019):3427–3437. doi:10.1039/C9LC00575G
19. Halámek J, Hepel M, Skládal P. Investigation of highly sensitive piezoelectric immunosensors for 2,4-dichlorophenoxyacetic acid. *Biosens Bioelectron*. 2001;16(2001):253–260. doi:10.1016/S0956-5663(01)00132-4
20. Zhang Y, Li Y, Wu W, Jiang Y, Hu B. Chitosan coated on the layers' glucose oxidase immobilized on cysteamine/Au electrode for use as glucose biosensor. *Biosens Bioelectron*. 2014;60:271–276. doi:10.1016/j.bios.2014.04.035
21. Gao S, Guisán JM, Rocha-Martin J. Oriented immobilization of antibodies onto sensing platforms - A critical review. *Anal Chim Acta*. 2022;1189 (2022):338907. doi:10.1016/j.aca.2021.338907
22. Ma H, He J, Zhu Z, et al. A quartz crystal microbalance-based molecular ruler for biopolymers. *Chem Commun*. 2010;46(6):946–951. doi:10.1039/B919179H
23. Sauerbrey GZ. Use of quartz crystal vibrator for weighting thin films on a microbalance. *Eur Phys J A*. 1959;155:206–222.
24. Zhang H, Jia Z, Wu C, et al. In vivo capture of circulating tumor cells based on transfusion with a vein indwelling needle. *ACS Appl Mater Interfaces*. 2015;7(36):20477–20484. doi:10.1021/acsami.5b06874
25. Sivagnanam V, Song B, Vandevyver C, Bünzli JC, Gijs MA. Selective breast cancer cell capture, culture, and immunocytochemical analysis using self-assembled magnetic bead patterns in a microfluidic chip. *Langmuir*. 2010;26(9):6091–6096. doi:10.1021/la9045572